

Study of copper(II) complexes of two diacetyl monooxime thiosemicarbazones: X-ray crystal structure and magneto-structural correlation of $[\text{Cu}(\text{dmoTSC})\text{Cl}]_2 \cdot \text{H}_2\text{O}$ (dmoTSC = monoanion of diacetyl monooxime thiosemicarbazone)

Sumita Naskar^a, Subhendu Naskar^{a,c}, Heike Mayer-Figge^b, William S. Sheldrick^b, Montserrat Corbella^{d,*}, Javier Tercero^d, Shyamal Kumar Chattopadhyay^{a,*}

^a Department of Chemistry, Bengal Engineering and Science University, Shibpur, Howrah 711 103, India

^b Lehrstuhl für Analytische Chemie, Ruhr-Universität Bochum, D-44780 Bochum, Germany

^c Department of Applied Chemistry, Birla Institute of Technology, Mesra, Ranchi 835215, Jharkhand, India

^d Department of Inorganic Chemistry, University of Barcelona, Martí i Franquès 1-11, 08028 Barcelona, Spain

ARTICLE INFO

Article history:

Received 26 October 2011

Accepted 31 December 2011

Available online 16 January 2012

Keywords:

Thiosemicarbazone
Diacetyl monooxime
Cu(II) complex
X-ray crystal structure
Magnetic interaction
DFT calculations

ABSTRACT

Cu(II) complexes of the tridentate thiosemicarbazone ligands diacetyl monooxime thiosemicarbazone (dmoTSC_2) and diacetyl monooxime (4-phenyl)thiosemicarbazone (dmoPhTSC_2) have been synthesized. X-ray crystal structures of dmoPhTSC_2 and $[\text{Cu}(\text{dmoTSC})\text{Cl}]_2 \cdot \text{H}_2\text{O}$ ($1 \cdot \text{H}_2\text{O}$) are also reported. The Cu(II) compound $1 \cdot \text{H}_2\text{O}$ is a dinuclear complex, where the Cu(II) centers have a square pyramidal geometry and are bridged by two thiolato ligands. A C_2 axis passes through the middle of Cu_2S_2 rectangle. Variable temperature susceptibility measurement for $1 \cdot \text{H}_2\text{O}$ shows that this compound exhibits a very weak antiferromagnetic behavior (in the solid state) with $J_1 = -2.97 \text{ cm}^{-1}$, using the Heisenberg isotropic spin Hamiltonian ($H = -J_1 S_1 \cdot S_2$). DFT calculations show that the intramolecular magnetic interaction should be ferromagnetic, and the net antiferromagnetic behavior is due to competition with antiferromagnetic intermolecular interactions through hydrogen bonds.

© 2012 Elsevier Ltd. All rights reserved.

1. Introduction

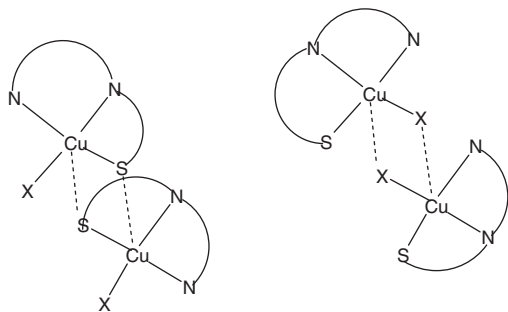
The coordination chemistry of Cu(II) with nitrogen–sulfur donor ligands remains an area of unabated attention due to their relevance to the active sites of various copper containing enzymes [1]. As a class of nitrogen–sulfur donor ligands, thiosemicarbazones are especially attractive because of the interesting chemical, biological, structural and electronic properties of their metal complexes [2–8]. It has also been known for a long time that Cu(II) thiosemicarbazone complexes possess cytotoxic and antitumor properties, and the biological activity of the thiosemicarbazones is enhanced on complexation to the Cu(II) ion [4,5,8–12]. A recent discovery of selective uptake and accumulation of certain bis(thiosemicarbazone)Cu(II) complexes by hypoxic malignant cells and the possible application of this phenomena for imaging of tumor cells by Positron Emission Tomography using ^{64}Cu (or other positron emitting radionuclides of copper, such as ^{60}Cu , ^{61}Cu or

^{62}Cu) has renewed interest in the study of the Cu(II) thiosemicarbazone complexes and their redox activities [12–16]. It is believed that reduction of Cu(II) to Cu(I) species is responsible for the accumulation of the copper thiosemicarbazone complexes inside the tumor cells.

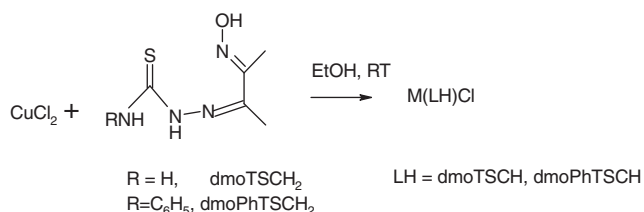
Most of the studies on Cu(II) thiosemicarbazone chemistry involve tridentate ligands like pyridine-2-aldehyde thiosemicarbazone and related derivatives or tetradentate ligands like diacetyl thiosemicarbazone or its derivatives [9–19]. Apart from their biological relevance, magneto-structural correlations of binuclear Cu(II) complexes of the type $[\text{CuLX}]_2$, where L is a tridentate thiosemicarbazone monoanion and X is a monoanionic donor, have also attracted considerable attention. In these binuclear complexes the Cu(II) atoms may be bridged by an enethiolato sulfur atom or by the X atoms (Scheme 1) [17–19]. In spite of considerable efforts, the factors that govern nature of the bridging atom (i.e. thiolato bridged versus X-bridged dimers) and the effects of various parameters, like bridge-angle, nature of coligands, extent of distortion of the coordination geometry of Cu(II) (from an ideal square planar arrangement) on the magnetic properties of the complexes are still not well understood. Diacetyl monooxime thiosemicarbazones (Scheme 2) have been shown to be versatile tridentate ligands

* Corresponding authors. Fax: +34 934907725 (M. Corbella), tel.: +91 33 2668 0521; fax: +91 33 2668 2916 (S.K. Chattopadhyay).

E-mail addresses: montse.corbella@ub.edu (M. Corbella), shch20@hotmail.com (S.K. Chattopadhyay).



Scheme 1.



Scheme 2.

[20–22], though their structural chemistry and magneto-structural correlations of their complexes are scarcely explored. We are particularly interested in these types of ligands because of the well known capability of the oxime moiety to form polynuclear complexes and its potential for generating interesting supramolecular networks [23–27]. The hydrogen atom of the oxime –OH group can participate in strong intra- or intermolecular hydrogen bond formations with other donor atoms or groups [21,22,28,29]. Thus metal complexes bearing non-deprotonated oximes may be considered as supramolecular synthons, capable of forming extended supramolecular networks via intermolecular hydrogen bonds. Moreover, such an extended hydrogen bonding network may act as a conduit for magnetic exchange between metal centers [30–32].

In this paper we report two Cu(II) complexes of thiosemicarbazone ligands formed by condensation of diacetyl monooxime with thiosemicarbazone or 4-(phenyl) thiosemicarbazone (Scheme 2). The X-ray crystal structures of one of the thiosemicarbazone ligands and one Cu(II) complex are also reported here. The magnetic properties of the structurally characterized Cu(II) complex is studied in details. An attempt is made to correlate the magneto-structural properties of our complex with those of similar complexes reported in the literature.

2. Experimental

2.1. Materials

CuCl₂·2H₂O, thiosemicarbazide and diacetyl monooxime were procured from Aldrich and were used without further purification. HPLC grade DMF and DMSO were used for spectroscopic and electrochemical studies. Tetraethyl ammonium perchlorate (TEAP) used for the electrochemical work was prepared as reported in the literature [33]. All solvents were of A.R. grade and were used as received for the synthetic work.

2.2. Physical measurements

Elemental analyses were performed on a Perkin-Elmer 2400 C, H, N analyzer. Infrared spectra were recorded as KBr pellets on a

JASCO FT-IR-460 spectrophotometer. UV–Vis spectra were recorded using a JASCO V-530 UV–Vis spectrophotometer. Electrochemical data were collected using a CH instruments 1106A potentiostat. A three-electrode configuration with Pt working and auxiliary electrodes, Ag/AgCl reference electrode were used. The potentials were calibrated against the ferrocene/ferrocenium couple (0.44 V versus Ag/AgCl reference). All the electrochemical experiments were performed under a dry nitrogen atmosphere with millimolar concentrations of the samples dissolved in DMSO containing 0.1 M TEAP as the supporting electrolyte.

Magnetic susceptibility measurements were carried out on a polycrystalline sample at the “Unitat de Mesures Magnètiques” (Universitat de Barcelona) with a Quantum Design SQUID MPMP-XL susceptometer apparatus, working in the range 2–300 K under magnetic fields of approximately 500 G (between 2 and 30 K) and 10000 G (between 35 and 300 K). Diamagnetic corrections were estimated from Pascal tables. The fit was performed by minimizing the function $R = \sum(\chi_M \cdot T_{\text{exp}} - \chi_M \cdot T_{\text{calc}})^2 / \sum(\chi_M \cdot T_{\text{exp}})^2$. X-band EPR spectra, on a polycrystalline sample, was recorded on a Bruker ESP-300E spectrometer, at room temperature and 70 K, at the “Unitat de Mesures Magnètiques” (Universitat de Barcelona).

2.3. Synthesis of the thiosemicarbazone ligands

The ligands diacetylmonooxime thiosemicarbazone (**dmotSCH₂**) and diacetylmonooxime (4-phenyl)thiosemicarbazone (**dmoPhTsch₂**) were prepared following the procedures described in the literature [20,34].

2.3.1. **dmotSCH₂**

Anal. Calc. for C₅H₁₀N₄SO: C, 34.48; H, 5.75; N, 32.18. Found: C, 34.51; H, 5.80; N, 32.24%. ¹H NMR (δ ppm): 11.56 (1H, s), 10.19 (1H, s), 8.34 (1H, s), 7.74 (1H, s), 2.09 (3H, s), 1.99 (3H, s). Selected IR bands (cm⁻¹): 3415 ν_{OH}, 3235 ν_{NH₂}^{as}, 3154 ν_{NH₂}^s, 1597 (ν_{C=N}), 1013 (ν_{N-O}), 780 (ν_{C=S}).

2.3.2. **dmoPhTsch₂**

Anal. Calc. for C₁₁H₁₄N₄SO: C, 52.80; H, 5.60; N, 22.40. Found: C, 52.65; H, 5.80; N, 22.58%. ¹H NMR (δ ppm): 11.66 (1H, s), 10.58 (1H, s), 9.88 (1H, s), 7.56 (2H, d), 7.36 (2H, t), 7.20 (1H, t), 2.17 (3H, s), 2.08 (3H, s). Selected IR bands (cm⁻¹): 3271 ν_{OH}, 3206 ν_{NH}, 1593 (ν_{C=N}), 1009 (ν_{N-O}), 758 (ν_{C=S}).

2.4. Synthesis of the complexes

2.4.1. Synthesis of [Cu(dmotSCH)Cl]₂·H₂O (1·H₂O)

To a solution of 0.171 g (1 mmol) CuCl₂·2H₂O in 10 mL ethanol was added a solution of 0.175 g (1 mmol) **dmotSCH₂** in 10 mL ethanol. A green precipitate separated out immediately. The pH of the reaction mixture was 3–4. After 1 h of stirring, concentrated HCl was added to the reaction mixture to adjust the pH to 1 and the resulting mixture was stirred for another 3 h. The green precipitate that formed was filtered, washed with alcohol and then dried over fused CaCl₂. The compound was recrystallized from ethanol. Yield: 0.120 g, 43%. *Anal. Calc.* for C₁₀H₂₀N₈S₂O₃Cl₂Cu₂: C, 21.33; H, 3.55; N, 19.91. Found: C, 21.52; H, 3.73; N, 19.98%. Electronic spectrum in DMF solution λ/nm (ε/M⁻¹ cm⁻¹): 626 (232), 404 (6445), 303 (23465). ESI-MS: 472 (100%) [M–2Cl–2H]⁺. Selected IR bands (cm⁻¹): 3227 (ν_{OH}), 3224 (ν_{NH₂}^{as}), 3140 (ν_{NH₂}^s), 1610 (ν_{C=N}), 1074 (ν_{N-O}).

2.4.2. [Cu(dmoPhTsch)Cl]₂ (2)

This was synthesized following a similar procedure to that of **1·H₂O**. Yield: 0.250 g, 67%. *Anal. Calc.* for C₂₂H₂₆N₈S₂O₂Cl₂Cu₂: C, 37.93; H, 3.73; N, 16.09. Found: C, 37.76; H, 3.76; N, 16.13%. Electronic spectrum in DMF solution λ/nm (ε/M⁻¹ cm⁻¹): 608 (568),

Table 1
Crystallographic data for **dmoPhTSCCH₂** and **[Cu(dmoTSCCH)Cl]₂·H₂O (1·H₂O)**.

	dmoPhTSCCH₂	1·H₂O
Empirical formula	C ₁₁ H ₁₄ N ₄ O ₅	C ₁₀ H ₁₈ Cl ₂ Cu ₂ N ₈ O ₂ S ₂ H ₂ O
<i>M</i>	250.33	562.48
<i>T</i> (K)	108 (2)	108 (2)
<i>λ</i> (Å)	0.71073	0.71073
Crystal system	monoclinic	monoclinic
Space group	<i>P</i> 2 ₁ / <i>n</i> (no. 14)	<i>C</i> 2/ <i>c</i>
<i>a</i> (Å)	5.4867(1)	10.5688(8)
<i>b</i> (Å)	22.1337(6)	14.5778(8)
<i>c</i> (Å)	9.9385(3)	12.9759(8)
<i>α</i> (°)	90	90
<i>β</i> (°)	92.723(3)	90.039(8)
<i>γ</i> (°)	90	90
<i>U</i> (Å ³), <i>Z</i>	1205.58(5), 4	1999.2(2), 4
<i>D</i> _{calc} (g cm ⁻³)	1.379	1.869
<i>μ</i> (mm ⁻¹)	0.258	2.633
Reflections collected		
Total, unique	10756, 2182	4572, 1876
<i>R</i> _{int}	0.029	0.070
Obs. (<i>I</i> > 2.0σ(<i>I</i>))	1713	1010
<i>R</i> ₁ (<i>I</i> > 2.0σ(<i>I</i>))	0.0305	0.0339
<i>wR</i> ₂ (all data)	0.0831	0.0550
Data/restraints/parameter	2182/0/156	1876/1/128
Goodness-of-fit (GOF) on <i>F</i> ²	1.01	0.69
Largest difference in peak and hole (e Å ⁻³)	0.25, -0.17	0.69, -0.38

414 (7950), 350 (10591). ESI-MS: 624 (98%) [M–2Cl–2H]⁺. Selected IR bands (cm⁻¹): 3317 (ν_{NH}), 1597 (ν_{C=N}), 1067 (ν_{N–O}).

2.5. Crystallographic data collection and structure determination

Crystal data were collected on a Bruker Smart CCD area detector diffractometer at 108(2) K for the ligand **dmoPhTSCCH₂** and the complex **1·H₂O**, using graphite-monochromated MoKα radiation. The structures were solved by direct methods and refined by least squares using the program SHELX 97 [35]. The non-hydrogen atoms were refined with anisotropic displacement parameters. All hydrogen atoms were placed at calculated positions and refined as riding atoms using isotropic displacement parameters coupled to those of the parent atoms. Semi-empirical absorption corrections along with corrections for the Lorentz and polarization effects were applied. A summary of the crystallographic data is collected in Table 1, and the important bond distances and angles are collected in Table 2.

2.6. Computational details

The computational strategy followed to calculate the exchange coupling constants in transition metal complexes was described in a previous paper [36]. For the calculation of the exchange coupling constants for any polynuclear complex with *n* different exchange constants, at least the energy of *n* + 1 spin configurations must be calculated. In the case of the studied models, we have calculated the energy corresponding to three or two different spin distributions to obtain two or one exchange coupling constants. The calculations were performed with the GAUSSIAN03 [37] program using guess functions generated with Jaguar 6.0 software [38]. The hybrid B3LYP functional [39] has been used in all calculations. We have employed a triple-ζ all electron basis set with two p polarization functions for copper atoms [40] and a double-ζ all electron basis set for the other elements, as proposed by Schaefer et al. [41].

3. Results and discussion

3.1. Synthesis

The Cu(II) compounds were obtained in good yields by the reaction of the appropriate thiosemicarbazone ligand with CuCl₂·2H₂O

Table 2
Selected bond distances (Å) and angles (°) for **dmoPhTSCCH₂** and **[Cu(dmoTSCCH)Cl]₂·H₂O (1·H₂O)**.

	1·H₂O	1·H₂O	dmoPhTSCCH₂
Cu(1)–N(1)	2.005(4)	S(1)–C(3)	1.760(5)
Cu(1)–N(2)	1.965(4)	O(1)–N(1)	1.386(5)
Cu(1)–Cl(1)	2.2434(13)	N(1)–C(1)	1.293(6)
Cu(1)–S(1)	2.2691(12)	N(2)–N(3)	1.378(5)
Cu(1)–S(1) ^d	2.8346(12)	N(2)–C(2)	1.290(6)
		N(3)–C(3)	1.321(5)
		N(4)–C(3)	1.333(5)
		N(4)–C(4)	1.416(2)
Cl(1)–Cu(1)–S(1)	102.43(5)	O(1)–N(1)–C(1)	116.7(3)
Cl(1)–Cu(1)–N(1)	93.74(13)	N(3)–N(2)–C(2)	119.3(4)
Cl(1)–Cu(1)–N(2)	167.12(12)	N(2)–N(3)–C(3)	112.2(3)
Cl(1)–Cu(1)–S(1) ^d	93.15(4)	N(1)–C(1)–C(2)	113.3(4)
S(1)–Cu(1)–N(1)	163.11(13)	N(2)–C(2)–C(1)	113.9(5)
S(1)–Cu(1)–N(2)	84.70(13)	S(1)–C(3)–N(3)	125.2(3)
S(1)–Cu(1)–S(1) ^d	95.74(4)	S(1)–C(3)–N(4)	117.0(3)
N(1)–Cu(1)–N(2)	78.51(17)	N(3)–C(3)–N(4)	117.8(4)
N(1)–Cu(1)–S(1) ^d	88.11(11)		
N(2)–Cu(1)–S(1) ^d	96.83(12)		
Cu(1)–S(1)–Cu(1) ^d	84.14(4)		

^d 2–*x*, *y*, 1/2–*z*.

in ethanol. The analytical data support their formulations. The IR spectra of the complexes indicate coordination through the deprotonated thiolate and the two imine nitrogen atoms. The structure of one Cu(II) complex was solved to get a better understanding of the molecular and supramolecular structures.

3.2. Description of the X-ray crystal structures

The ORTEP diagram for the ligand **dmoPhTSCCH₂** is given in Fig. 1. In the free ligand **dmoPhTSCCH₂** (Fig. 1) the N2 atom is trans to both S1 and N1 atoms. The iminooxime thiosemicarbazone backbone is planar and it makes a dihedral angle of 9.41(6)° with the phenyl ring. The observed bond lengths are similar to those reported in the literature [34] and reflect π-delocalization over the thiosemicarbazone backbone. In the lattice, two adjacent molecules form a complementary hydrogen bonded dimer by O(1)–H(1)···N(1)^a interactions (symmetry code for a = 2–*x*, –*y*, –*z*; see Table 3 for details of the H-bonding parameters). These dimers are then interlinked with each other by complementary N(3)–H(3)···S(1)^b (symmetry code for b = –*x*, –*y*, 1–*z*) hydrogen bonds, forming two dimensional sheets (Supplementary Fig. 1). Adjacent sheets are then interconnected to each other by complementary C(21)–H(21C)···O(1)^c interactions (symmetry code for c = 1–*x*, –*y*, –*z*) to form a three dimensional network (Supplementary Fig. 2).

The asymmetric unit of **[Cu(dmoTSCCH)Cl]₂·H₂O** (Fig. 2) consists of a square plane around the central Cu(II) atom, which is coordinated to the iminooxime nitrogen (N1), imine nitrogen (N2), deprotonated iminothiolate sulfur (S1) and the chloride ion (Cl1); half a molecule of lattice water completes the asymmetric unit. The dihedral angle between the two chelate rings is 3.11(6)°. The ligand is effectively planar, but the S(1), Cu(1) and Cl(1) atoms deviate from the plane of the ligand by 0.250(1), 0.181(1) and –0.033(1) Å, respectively. Apart from the N(1), N(2), S(1) and Cl(1) atoms, which constitute the square plane around the Cu(1) atom, another sulfur atom (S(1)^d, symmetry code for d = 2–*x*, *y*, 1/2–*z*) of a neighboring asymmetric unit is also coordinated to the Cu(1) atom at a longish distance of 2.8346(12) Å, making the Cu(II) coordination environment square pyramidal (τ = 0.07) [42]. The Cu(1)^d atom of the same neighboring unit is similarly bonded to the S(1) atom of the first unit, forming a dinuclear complex (Fig. 3). The basal planes of the two square pyramidal Cu(II)

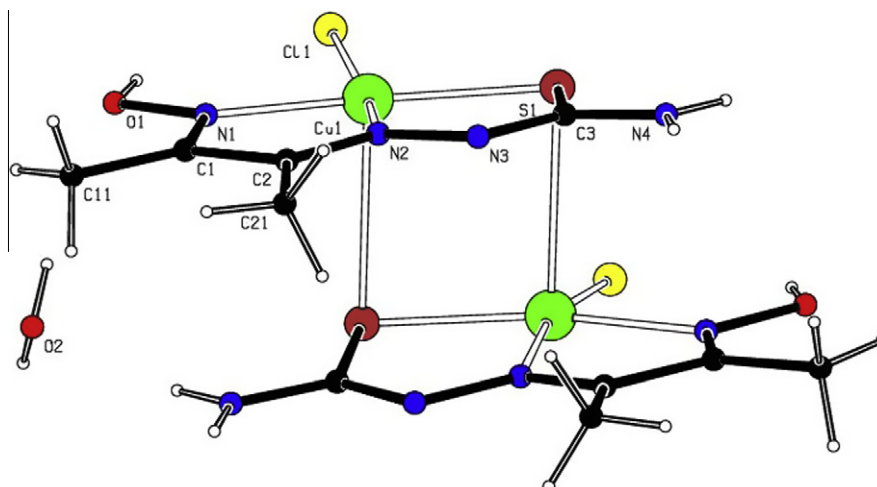


Fig. 3. The dimeric structure of $[\text{Cu}(\text{dmoTSCH})\text{Cl}]_2 \cdot \text{H}_2\text{O}$ ($1 \cdot \text{H}_2\text{O}$).

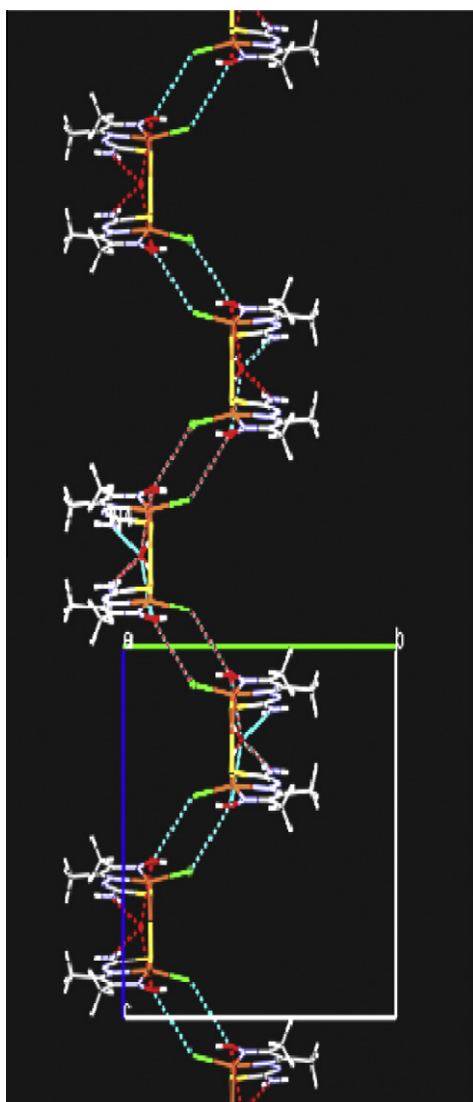


Fig. 4. One dimensional zig-zag chain of $1 \cdot \text{H}_2\text{O}$ along 'c' axis.

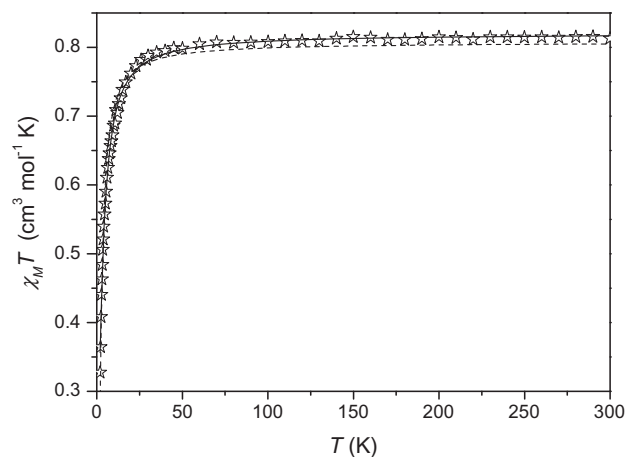


Fig. 5. $\chi_M T$ vs. T plot for compound $[\text{Cu}(\text{dmoTSCH})\text{Cl}]_2 \cdot \text{H}_2\text{O}$ ($1 \cdot \text{H}_2\text{O}$). The \star symbol represents the experimental values and the dashed line and solid line represent the best fit with the equation for a dinuclear complex and including the intermolecular interactions, respectively.

some derivatives of it as a polydentate ligand and consequently the basal plane is constituted by CuXN_2S . The same basal plane is also

present in compound **1**, though the tridentate monoanionic thiosemicarbazone ligand is slightly different. As a result, the structural parameters of the present compound are comparable to those reported for the other compounds in Table 4. In contrast, compound **E**, $[\text{Cu}_2\text{Cl}_2(\mu\text{-S-dept})_2][\text{Cu}_2\text{Cl}_4(\mu\text{-Cl})_2]$ with the S-dept (S-dept = $(N,N,N',N'$ -tetraethyl) pyridine-2,6-dithiocarboxamide) ligand [44], has two sulfur atoms in the basal plane (CuXNS_2) and its structural parameters are significantly different from the values found for the other compounds in Table 4. So except for compound **E**, the values of the structural parameters for the other compounds are of the same order, with some variation in the $\text{Cu-S}_{\text{apical}}$ distance (2.74–2.92 Å) and the Cu-S-Cu angle (85.5–99.79°); however, in spite of these similarities, the magnetic behavior is significantly different, with values in the range -28.1 to $+13.8 \text{ cm}^{-1}$. It was reported by Garcia-Torjal and co-workers [17], that the nature of the coligands in the basal plane influences the magnetic behavior. The most antiferromagnetic coupling was found for compounds where X has a low electronegativity value ($X = \text{I}$), while the most ferromagnetic coupling values were found for compounds where the electronegativity of X was high ($X = \text{O}$). However, when the monodentate ligand (X) is polyatomic, donating through an O atom, the reported compounds (Table 4) could

Table 4

Comparison of structural parameters and the magnetic exchange constant J ($H = -JS_1 \cdot S_2$) for dinuclear complexes with a $[\text{Cu}_2(\mu\text{-S})_2]$ core, a square-pyramidal environment of the Cu(II) ions, sharing a base to apex edge, and a CuXYNS basal plane, where $Y = N$ except for *E* where $Y = S$.

	X	$d(\text{Cu}-\text{S}_b)^a$ (Å)	$d(\text{Cu}-\text{S}_a)^b$ (Å)	α (CuSCu) (°)	$d(\text{Cu} \cdots \text{Cu})$ (Å)	$J_1(\text{exp.})$ (cm^{-1})	Ref.
A	I	2.27	2.78	85.80	3.46	−28.1	[17]
B	Br	2.27	2.83	88.3	3.58	−12.3	[17]
C	Br	2.28	2.74	87.11	3.47	−9.4	[18]
D	Cl	2.28	2.76	87.01	3.49	−9.4	[18]
1-H₂O	Cl	2.27	2.84	84.14	3.44	−3.0	
E	Cl	2.28	3.42	91.72	4.17	−2.6	[44]
F	N _{SCN}	2.28	2.75	86	3.45	−10.2	[19]
G	O _{NO₂}	2.27	2.92	85.5	3.55	−6.8	[45]
H	O _{HCOO}	2.27	2.82	86.34	3.50	−5.6	[45]
I	O _{NO₃}	2.30	2.80	99.79		v. w. AF	[46]
J	O _{NO₃}	2.29	2.82	86.54	3.52	7.6	[47]
K	O _{NO₃}	2.27	2.77	85.83	3.45	13.8	[17,48]

^a This work. **A**: $\{[\text{Cu}(\text{L}_1)]_2\}$ (HL_1 = pyridine-2-carbaldehyde thiosemicarbazone); **B**: $\{[\text{Cu}(\text{L}_1\text{mm})\text{Br}]_2\}$ (HL_1mm = pyridine-2-carbaldehyde (N(4)-methyl) thiosemicarbazone); **C**: $\{[\text{CuBr}(\text{L}_1)]_2\}$; **D**: $\{[\text{CuCl}(\text{L}_1)]_2\}$; **E**: $[\text{Cu}_2\text{Cl}_2(\mu\text{-S-dept})_2][\text{Cu}_2\text{Cl}_4(\mu\text{-Cl})_2]$ (*S-dept* = (N,N,N',N'-tetraethyl) pyridine-2,6-dithiocarbamide); **F**: $\{[\text{Cu}(\text{NCS})(\text{L}_1)]_2\}$; **G**: $\{[\text{Cu}(\text{L}_1)(\text{NO}_2)]_2\}$; **H**: $\{[\text{Cu}(\text{L}_1)(\text{HCOO})]_2\}$; **I**: $[\text{Cu}(\text{mpsm})](\text{ONO}_2)$ (*Hmpsm* = 6-methyl-2-formylpyridine Schiff base of *S*-methylthiocarbazate); **J**: $[\text{Cu}_2(\text{L}_2)(\text{NO}_3)_2][\text{Cu}(\text{L})(\text{NO}_3)]$ (*HL* = 2-*S*-methyl-6-methyl-4-formyl pyrimidine-(N(4)-ethyl)-thiosemicarbazone); **K**: $\{[\text{Cu}(\text{L}_1\text{mm})\text{NO}_3]_2\}$.

^a $d(\text{Cu}-\text{S}_{\text{basal}})$.

^b $d(\text{Cu}-\text{S}_{\text{apical}})$.

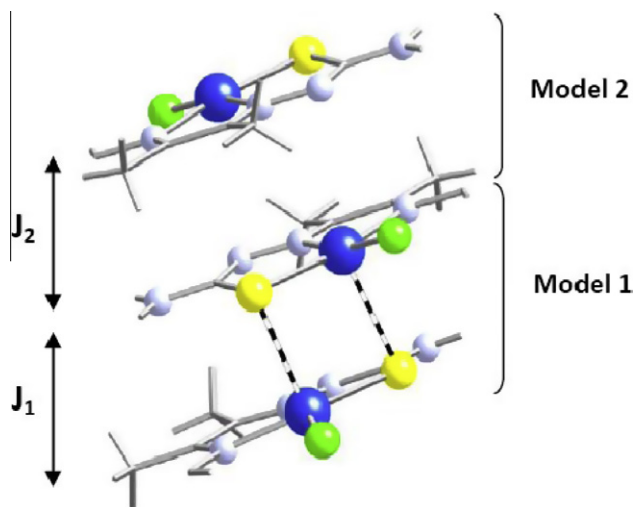


Fig. 6. Structural representation of the trinuclear model showing the exchange coupling constants J_1 and J_2 . Multiband cylinder bonds indicate the longer distance in dinuclear entity Cu–S (2.86 Å) (*model 1*).

show antiferromagnetic (**G**, **H**, **I**) or ferromagnetic (**J**, **K**) behavior. As was reported for other types of complexes, in some cases, the nitrate ligand could act as a π -acid ligand and as a consequence could decrease the antiferromagnetic contribution [49].

Compound **1-H₂O** shows a weak antiferromagnetic behavior, the coupling constant being smaller than those reported for the other compounds with monoatomic monodentate ligands (**A–D**). In this case the distortion of the square-pyramid towards trigonal bipyramid is negligible, and in consequence the overlap through the bridge must be very poor, and a ferromagnetic behavior is expected. With the aim of understanding the observed antiferromagnetic behavior, density functional calculations using the experimental coordinates of this compound were performed (*model 1*, Fig. 6) and the obtained J_1 value was $+5.0 \text{ cm}^{-1}$. This result, although in contradiction to the observed behavior, is expected due to the apical equatorial nature of the bridging atoms. It is necessary to take into consideration other factors to explain the experimental results.

In an attempt to understand the influence of the Cu–S distance on the exchange coupling parameter J_1 , we have varied this

distance in the range 2.3–3.0 Å. In all cases the calculated interaction is ferromagnetic, with J_1 values in the range $+33.1$ to $+3.0 \text{ cm}^{-1}$, for a shorter and longer distance, respectively. These results are in agreement with the calculations carried out previously for a similar compound reported in Ref. [47].

The sign of this interaction can be rationalized using the Hay–Thibeault–Hoffmann model [50]; the magnetic coupling constant can be expressed as a sum of two contributions, ferromagnetic and antiferromagnetic ones, $J = J_F + J_{AF}$. The quasi parallel disposition of the $d_{x^2-y^2}$ magnetic orbitals (basal planes of the square pyramid) can be translated in a poor overlap between these orbitals, and consequently the antiferromagnetic contribution must be close to zero, the ferromagnetic one dominating. As the angle between squares planes of the Cu(II) ions in the dinuclear compound is 2.5° , we can expect that due to shortening of the Cu–S distance, the antiferromagnetic term changes very little (poor overlap in all cases), while the ferromagnetic one increases, as we have found in the DFT calculation.

Thus, contrary to our experimental results, these calculations indicate that the magnetic interaction in the dinuclear complex must be ferromagnetic. As discussed in the X-ray crystal structure section, several hydrogen bonds are present in the lattice, intramolecular O–H \cdots Cl and intermolecular O–H \cdots Ow, N–H \cdots Ow and N–H \cdots Cl interactions, generating a 3D-network, which could provide pathways for the magnetic exchanges. Taking into account these facts, we selected four additional models from the crystal structure data to analyze independently each interaction. *Model 2* (Fig. 6) considers the stacking between the dinuclear complexes; for the calculation of the magnetic exchange in this direction (J_2), only one [CuLCl] fragment of each dinuclear complex was considered. *Model 3* considers the interaction of two dinuclear complexes through the hydrogen bonds with the water molecule (J_3) (Fig. 7). *Model 4* analyzes the effect of the Cl \cdots H–N hydrogen bond interaction (J_4) (Fig. 8), and *model 5* the effect of the Cl \cdots O interaction (J_5) (Fig. 9). As in the case of *model 2*, the calculations for other models also were performed using only one [CuLCl] fragment of each dinuclear complex. The magnetic coupling constants calculated with each model (J_2 , J_3 , J_4 and J_5) correspond to the intermolecular exchange pathways, while J_1 describes the intra-dimer interaction in the dinuclear complex, which, as already indicated above, is ferromagnetic ($J_1 = +5.0 \text{ cm}^{-1}$).

For all models, we have obtained small negative values, indicative of antiferromagnetic contributions. The calculated values are,

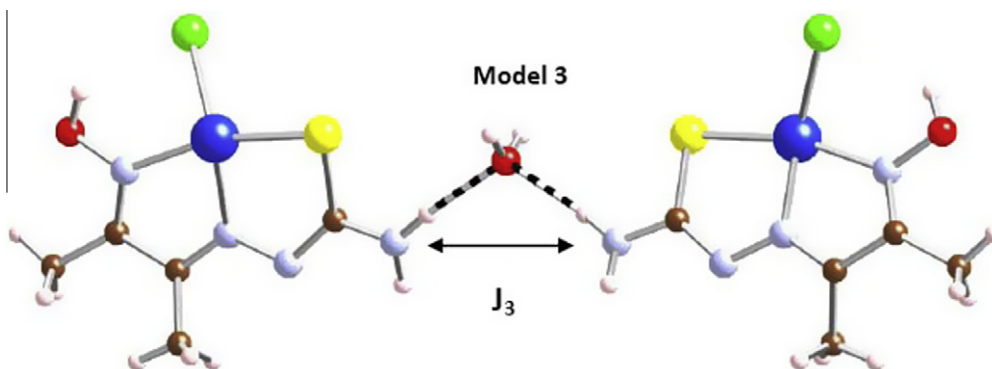


Fig. 7. Molecular structure representation and exchange coupling constant (J_3) of dinuclear entity connected via hydrogen bonds. Multiband cylinder bonds indicate the hydrogen bond ($\text{H}\cdots\text{O}\cdots\text{H}$) in the dinuclear model.

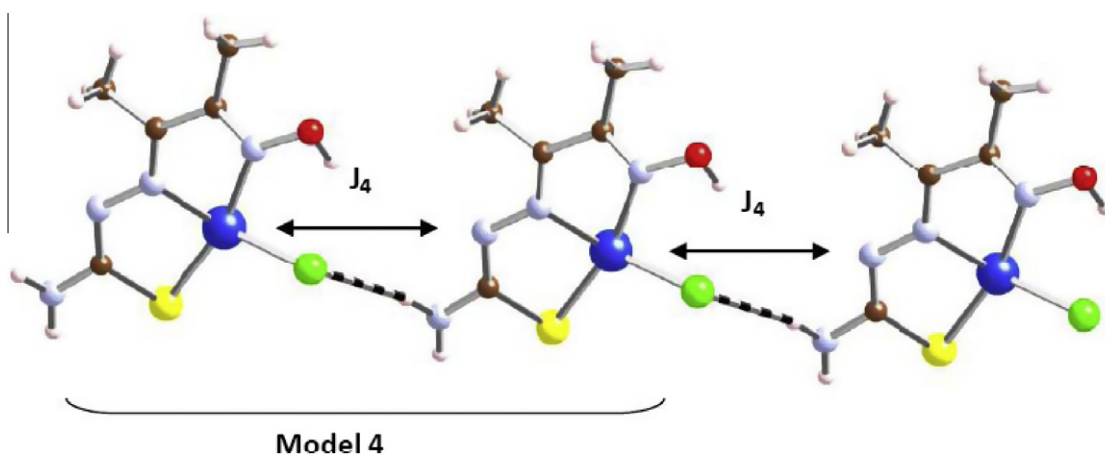


Fig. 8. Structural representation of the trinuclear model showing the exchange coupling constant J_4 between dinuclear entities (*model 4*). Multiband cylinder bonds indicate the $\text{Cl}\cdots\text{H}$ hydrogen bonds between the adjacent copper monomers.

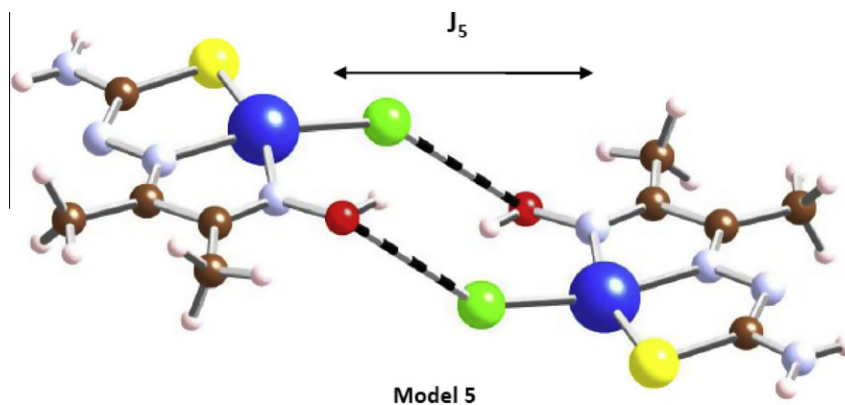


Fig. 9. Molecular structure representation and exchange coupling constant (J_5) of dinuclear entity connected via $\text{Cl}\cdots\text{O}$ contacts. Multiband cylinder bonds indicate the $\text{Cl}\cdots\text{O}$ contacts in the dinuclear entity.

$J_2 = -0.4 \text{ cm}^{-1}$, $J_3 = -0.1 \text{ cm}^{-1}$, $J_4 = -3.8 \text{ cm}^{-1}$ and $J_5 = -2.1 \text{ cm}^{-1}$. The magnetic behavior for this compound must be the sum of all the interactions: intramolecular ($J_1 = +5.0 \text{ cm}^{-1}$) and intermolecular ($J_2 + J_3 + J_4 + J_5 = -6.4 \text{ cm}^{-1}$), which gives a net antiferromagnetic coupling. This result is in agreement with the sign of the coupling constant found fitting the experimental data (-2.97 cm^{-1}).

As it was indicated, the calculations carried out with these models considered only two $[\text{CuLCl}]$ fragments of different entities. In

order to evaluate the effect of the nuclearity in the previous J_i values we carried out two new calculations, with three $[\text{CuLCl}]$ fragments (trinuclear models):

- (a) A modification of *model 1* and *model 2*: We considered one dinuclear complex, with J_1 , and their interaction with the $[\text{CuLCl}]$ fragment of a neighbor stacked dinuclear complex, with a J_2 interaction (Figs. 6 and 10).

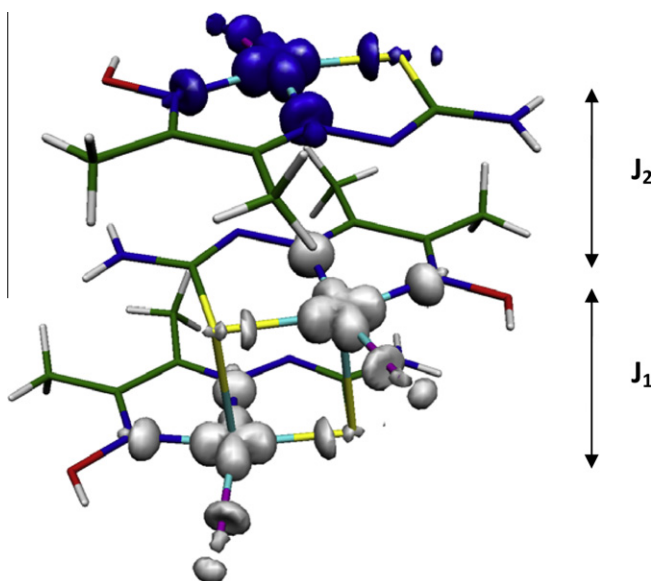


Fig. 10. Spin-density distribution for trinuclear model corresponding to the $S = 1/2$ ground-state single-determinant B3LYP solution. Positive and negative values are represented as white and dark surfaces, respectively.

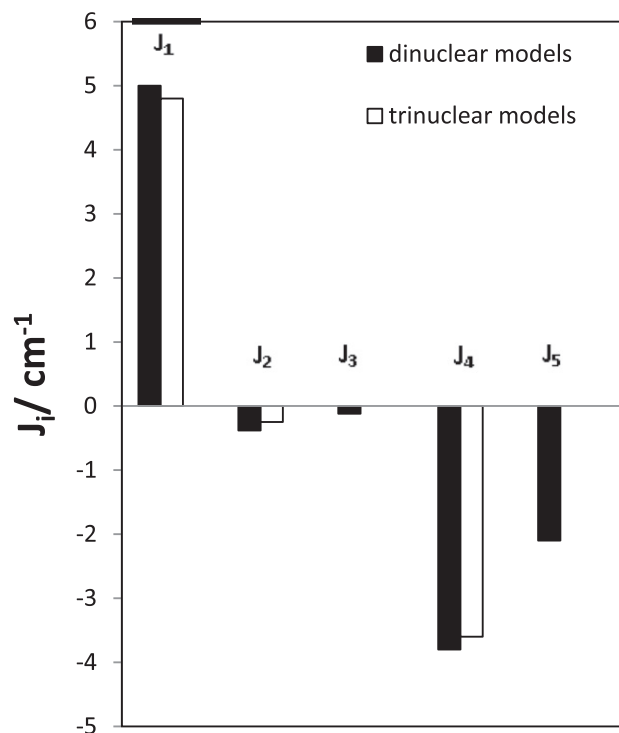


Fig. 11. Calculated DFT values of the different types of exchange coupling constants for $1\text{-H}_2\text{O}$ and the variation of these values considering the nuclearity of the models studied (see text).

(b) A modification of *model 4*: In this case we considered three $[\text{CuLCl}]$ fragments of three neighboring dinuclear complexes, with a J_4 interaction between them (Fig. 8).

The J_1 , J_2 and J_4 values obtained with these models (trinuclear models) are basically the same as those found with the dinuclear models (*models 1,2,4*), with a decrease between 0.1 and 0.3 cm^{-1} (Fig. 11). Therefore, the dinuclear models are a good approach to

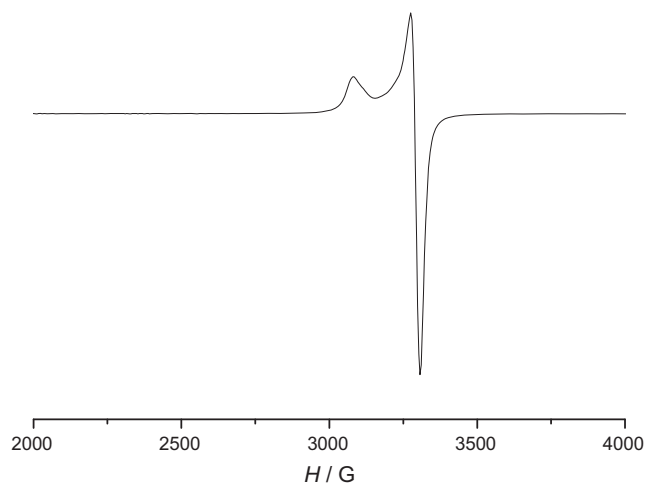


Fig. 12. X-band EPR spectrum, on polycrystalline sample of $1\text{-H}_2\text{O}$, at 70 K.

Table 5

Experimental EPR parameters for compounds with a $[\text{Cu}_2(\mu\text{-S})_2]$ core and square-pyramidal environment of the Cu(II) ions, sharing a base to apex edge.

	g_{iso}	g_{\parallel}	g_{\perp}	g_1	g_2	g_3	Ref.
A	2.074						[17]
B				2.152	2.043	2.031	[17]
C				2.161	2.057	2.033	[18]
D				2.183	2.053	2.033	[18]
1-H₂O		2.18	2.05				
E		2.17	2.07				[44]
F				2.148	2.064	2.040	[19]
G				2.183	2.037	2.029	[45]
H				2.186	2.046	2.038	[45]
I		2.2215	2.054				[46]
J	2.09						[47]
K				2.186	2.049	2.025	[17,48]

^a This work.

explain the different magnetic exchange pathways present in the compound $1\text{-H}_2\text{O}$.

From these results we can conclude that the experimental anti-ferromagnetic behavior is due to the combination of two interactions having opposite signs for J values: a ferromagnetic $\text{Cu}\cdots\text{Cu}$ interaction through the sulfur atom in the dinuclear complex and antiferromagnetic interactions due to the hydrogen bonds between dinuclear complexes. The most important antiferromagnetic contributions are the J_4 and J_5 coupling constants, revealing the importance of the Cl^- ligands in the magnetic properties (Figs. 8, 9 and 11).

Taking into consideration these results, we performed a new fit of the experimental data with the Bleaney–Bowers equation [43], considering the intramolecular ferromagnetic interaction (J_1) and including the overall intermolecular interactions with a single parameter (J') [51]. The best fit was obtained with $J_1 = 4.79 \text{ cm}^{-1}$, $J' = -4.29 \text{ cm}^{-1}$ and $g = 2.09$ ($R = 9.28 \times 10^{-5}$) (solid line in Fig. 5). This result agrees with the conclusions from the DFT calculations, showing the observed weak antiferromagnetic behavior is due to the competition between the ferromagnetic interaction within the dinuclear complex and the antiferromagnetic interactions between the dinuclear complexes.

The X-band EPR spectrum of a polycrystalline sample is shown in Fig. 12. It shows two signals at $g_{\parallel} = 2.18$ and $g_{\perp} = 2.05$, characteristic of Cu(II) ions in a square pyramidal environment. These values are similar to the reported values for analogous compounds (Table 5).

3.4. Electrochemistry

In the cyclic voltammetry experiments, the free ligand **dmoTSCH₂** shows no redox activity up to 1.0 V (versus Ag/AgCl) in DMSO with a Pt electrode. On the cathodic side, a quasi-reversible response is obtained at -0.81 V ($\Delta E_p = 280$ mV). In the corresponding Zn(II) complex, we could detect no oxidative response up to 1.0 V, but an irreversible reductive response is observed at -0.85 V. Very similar behavior is observed with the **dmoPhTSCH₂** ligand.

The Cu(II) complex **1·H₂O** in DMSO solution shows a Cu(III)/Cu(II) couple at 0.28 V (180 mV); two reductive peaks observed at -0.30 V (300 mV) and -1.13 V are assigned to the Cu(II)/Cu(I) couple and a ligand based reduction, respectively (Supplementary Figs. 5 and 6). The complex **2** in DMSO solution shows the Cu(III)/Cu(II) couple at 0.28 V (248 mV), while on the reductive side the Cu(II)/Cu(I) couple is observed at -0.26 (260 mV) and the ligand based reduction at -0.65 (100) V (Supplementary Fig. 7). It has been pointed out that Cu(II) thiosemicarbazone complexes having a reversible Cu(II)/Cu(I) potential around -0.5 to -0.6 V are hypoxia selective, and hence may be used as imaging agents of hypoxic tissues [15,16]. The E^0 values of the Cu(II)/Cu(I) couple of our complexes are more positive than the specified range mentioned above and hence they are not expected to show hypoxia selectivity.

3.5. Electronic spectra

The Cu(II) complexes show a weak band/shoulder around 600 nm, assigned to d–d transitions [19,52]. They also show a ligand to metal charge transfer transition at around 400 nm. Another band in the 300–350 nm region is due to an intraligand transition (Supplementary Figs. 8 and 9).

4. Conclusion

We have shown that diacetyl monooxime thiosemicarbazones are versatile ligands, capable of forming extended networks through hydrogen bonding which can act as a conduit for transmitting magnetic exchange interactions. With Cu(II) they form thiola-to bridged dinuclear complexes, where each Cu(II) is in a 4+1 coordination environment. The magnetic behavior of such complexes are shown to be a combined effect of intramolecular superexchange and intermolecular interactions through various types of hydrogen bonds. The possible substitution of chloride by other monodentate ligands, which will alter the hydrogen bonding pattern and hence the intermolecular interactions, as well as the intramolecular superexchange (which depends on the electronegativity of the donor atom X, vide supra) are now being explored in our laboratory.

Acknowledgments

SKC thanks AICTE, UGC and CSIR for financial assistance. Sumita thanks CSIR for a SRF. SKC also thanks Mr. Manas Ghosh for doing a part of the work during his PG project. We also acknowledge AICTE for funding the purchase of a CH1106A potentiostat. The infrastructural facility created in our department through DST-FIST, UGC-SAP and a MHRD special grant is also thankfully acknowledged. M. Corbella thanks the Ministerio de Educación y Ciencia (CTQ2009-07264/BQU and CTQ2008-06670C02-01/BQU) and to the Comissió Interdepartamental de Recerca i Innovació Tecnològica de la Generalitat de Catalunya (CIRIT) (2009-SGR1454 and 2009SGR1459) for financial support. J. Tercero is grateful to the Centre de Computació de Catalunya (CESCA) with a grant provided

by Fundació Catalana per a la Recerca (FCR) and the Universitat de Barcelona.

Appendix A. Supplementary data

CCDC 800029 and 800031 contain the supplementary crystallographic data for **dmoPhTSCH₂** and **[Cu(dmoTSCH)Cl]₂·H₂O (1·H₂O)**, respectively. These data can be obtained free of charge via <http://www.ccdc.cam.ac.uk/conts/retrieving.html>, or from the Cambridge Crystallographic Data Centre, 12 Union Road, Cambridge CB2 1EZ, UK; fax: (+44) 1223-336-033; or e-mail: deposit@ccdc.cam.ac.uk. Supplementary data associated with this article can be found, in the online version, at doi:10.1016/j.poly.2011.12.042.

References

- [1] J.A. McCleverty, T.J. Meyer (Series Eds.), *Comprehensive Coordination Chemistry-II*, vol. 8, in: L. Que, Jr., W.B. Tolman (Eds.), Elsevier, Amsterdam, 2005 (Chapters 8.1, 8.4, 8.17).
- [2] M.J.M. Campbell, *Coord. Chem. Rev.* 15 (1975) 279.
- [3] S. Padhye, G.B. Kauffman, *Coord. Chem. Rev.* 63 (1985) 127.
- [4] D.X. West, S.B. Padhye, P.B. Sonowane, *Struct. Bond.* 76 (1991) 1.
- [5] D.X. West, A.E. Liberta, S.B. Chikate, P.B. Sonowane, A.S. Kumbhar, R.G. Yerande, *Coord. Chem. Rev.* 123 (1993) 49.
- [6] T.S. Lobana, R. Sharma, G. Bawa, S. Khanna, *Coord. Chem. Rev.* 253 (2009) 977.
- [7] S.K. Chattopadhyay, in: D.B. Watson (Ed.), *Ruthenium: Properties, Production and Applications*, Nova Publishers, 2011, pp. 293–310.
- [8] D.H. Petering, *Bioinorg. Chem.* 1 (1972) 255.
- [9] M. Christlieb, H.S.R. Struthers, P.D. Bonnitche, A.R. Cowley, J.R. Dilworth, *Dalton Trans.* (2007) 5043.
- [10] H.G. Petering, H.H. Buskirk, G.B. Underwood, *Cancer Res.* 24 (1964) 367.
- [11] D.H. Petering, in: H. Sigel (Ed.), *Metal Ions in Biological Systems*, Marcel Dekker, New York, 1980, pp. 197–229.
- [12] J.P. Holland, J.C. Green, J.R. Dilworth, *Dalton Trans.* (2006) 783.
- [13] A.R. Cowley, J.R. Dilworth, P.S. Donnelly, A.D. Gee, J.M. Heslop, *Dalton Trans.* (2004) 2404.
- [14] J.L.J. Dearling, J.S. Lewis, D.W. McCarthy, M.J. Welch, P.J. Blower, *Chem. Commun.* (1998) 2531.
- [15] J.L.J. Dearling, J.S. Lewis, G.E.D. Mullen, M.J. Welch, P.J. Blower, *J. Biol. Inorg. Chem.* 7 (2002) 249.
- [16] A.R. Cowley, J.R. Dilworth, P.S. Donnelly, E. Labisbal, A. Sousa, *J. Am. Chem. Soc.* 124 (2002) 5270.
- [17] P. Gómez-Saiz, J. Garcia-Torjal, M.A. Maestro, J. Mahía, F.J. Arnaiz, L. Lezama, T. Rojo, *Eur. J. Inorg. Chem.* (2003) 2639.
- [18] J. Garcia-Torjal, M.K. Urtiaga, R. Cortés, L. Lezama, T. Rojo, M.I. Arriortua, *J. Chem. Soc., Dalton Trans.* (1994) 2233.
- [19] J. Garcia-Torjal, L. Lezama, J.L. Pizarro, M. Insausti, M.I. Arriortua, T. Rojo, *Polyhedron* 18 (1999) 3703.
- [20] S. Ghosh, P.K. Ray, S.R. Saha, A.P. Koley, *Ind. J. Chem.* 23A (1984) 745.
- [21] S.K. Chattopadhyay, D. Chattopadhyay, T. Banerjee, R. Kuroda, S. Ghosh, *Polyhedron* 16 (1997) 1925.
- [22] A.K. Das, S. Seth, S.K. Chattopadhyay, *Z. Kristallogr.* 215 (2000) 481.
- [23] S. Naskar, D. Mishra, R.J. Butcher, S.K. Chattopadhyay, *Polyhedron* 26 (2007) 3703.
- [24] S. Sreerama, S. Pal, *Inorg. Chem.* 41 (2002) 4843.
- [25] D. Datta, A. Chakravorty, *Inorg. Chem.* 21 (1982) 363.
- [26] S. Ross, T. Weyhermüller, E. Bill, E. Bothe, U. Flörke, K. Wieghardt, P. Chaudhuri, *Eur. J. Inorg. Chem.* (2004) 984.
- [27] S. Wan, W. Mori, S. Yamada, S.I. Murahashi, *Bull. Chem. Soc. Jpn.* 62 (1989) 435.
- [28] V.Y. Kukuskin, T. Nishioka, D. Tudela, K. Isobe, I. Kinoshita, *Inorg. Chem.* 36 (1997) 6157.
- [29] R.S. Bendre, R.J. Butcher, A.S. Kuwar, *Acta Crystallogr., Sect. E* 61 (2005) o3511.
- [30] H. Muhonen, *Inorg. Chem.* 25 (1986) 4692.
- [31] E. Escrivà, J.S. Carrió, J.G. Lozano, J.-V. Folgado, F. Sapiña, L. Lezama, *Inorg. Chim. Acta* 279 (1998) 58.
- [32] P.A. Goodson, J. Glerup, D.J. Hodgson, K. Michelsen, U. Rychlewski, *Inorg. Chem.* 33 (1994) 359.
- [33] D.T. Sawyer, A. Sobkowiak, J.L. Roberts Jr., *Electrochemistry for Chemists*, second ed., John Wiley and Sons, New York, 1995, p. 333.
- [34] A.K. Nandi, S. Chaudhuri, S.K. Majumder, S. Ghosh, *Acta Crystallogr., Sect. C* 40 (1984) 1193.
- [35] G.M. Sheldrick, SHELX97 [Includes SHELXS97, SHELXL97, CIFTAB], Program for Crystal Structure Analysis (Release 97-2), Göttingen, Germany, 1998.
- [36] E. Ruiz, *Struct. Bond.* 113 (2004) 71.
- [37] M.J. Frisch, G.W. Trucks, H.B. Schlegel, G.E. Scuseria, M.A. Robb, J.R. Cheeseman, J.A. Montgomery, T. Vreven, K.N. Kudin, J.C. Burant, J.M. Millam, S.S. Iyengar, J. Tomasi, V. Barone, B. Mennucci, M. Cossi, G. Scalmani, N. Rega, G.A. Petersson, H. Nakatsuji, M. Hada, M. Ehara, K. Toyota, R. Fukuda, J. Hasegawa, H. Ishida, T. Nakajima, Y. Honda, O. Kitao, H. Nakai, M. Klene, X. Li, J.E.; Knox, H.P.

- Hratchian, J.B. Cross, C. Adamo, J. Jaramillo, R. Gomperts, R.E. Stratmann, O. Yazyev, A.J. Austin, R. Cammi, C. Pomelli, J. Ochterski, P.Y. Ayala, K. Morokuma, G.A. Voth, P. Salvador, J.J. Dannenberg, V.G. Zakrzewski, S. Dapprich, A.D. Daniels, M.C. Strain, O. Farkas, D.K. Malick, A.D. Rabuck, K. Raghavachari, J.B. Foresman, J.V. Ortiz, Q. Cui, A.G. Baboul, S. Clifford, J. Cioslowski, B.B. Stefanov, G. Liu, A. Liashenko, P. Piskorz, I. Komaromi, R.L. Martin, D.J. Fox, T. Keith, M.A. Al-Laham, C.Y. Peng, A. Nanayakkara, M. Challacombe, P.M.W. Gill, B. Johnson, W. Chen, M.W. Wong, C. Gonzalez, J.A. Pople, Gaussian 03 (Revision B.4), Pittsburgh, PA, 2003.
- [38] Schrodinger Inc., 'Jaguar 6.0', Portland, 2005.
- [39] A.D. Becke, *J. Chem. Phys.* 98 (1993) 5648.
- [40] A. Schaefer, C. Huber, R. Ahlrichs, *J. Chem. Phys.* 100 (1994) 5829.
- [41] A. Schaefer, H. Horn, R. Ahlrichs, *J. Chem. Phys.* 97 (1992) 2571.
- [42] A.W. Addison, T.N. Rao, J. Reedijk, J.V. Rijn, G.C. Verschoor, *J. Chem. Soc., Dalton Trans.* (1984) 1349.
- [43] B. Bleaney, K.D. Bowers, *Proc. Roy. Soc. London, Ser. A* 214 (1952) 451.
- [44] R. Kapoor, A. Kataria, P. Venugopalan, P. Kapoor, M. Corbella, M. Rodríguez, I. Romero, A. Llobet, *Inorg. Chem.* 43 (2004) 6699.
- [45] P. Gómez-Saiz, J. García-Torjal, A. Mendia, B. Donnadieu, L. Lezama, J.L. Pizarro, M.I. Arriortua, T. Rojo, *Eur. J. Inorg. Chem.* (2003) 518.
- [46] M.A. Ali, A.H. Mirza, R.J. Fereday, R.J. Butcher, J.M. Fuller, S.C. Drew, L.R. Gahan, G.R. Hanson, B. Moubaraki, K.S. Murray, *Inorg. Chim. Acta* 358 (2005) 3937.
- [47] S. Gupta, S. Pal, A.K. Barik, A. Hazra, S. Roy, T.N. Mandal, S.-M. Peng, G.-H. Lee, M.S. El Fallah, J. Tercero, S.K. Kar, *Polyhedron* 27 (2008) 2519.
- [48] P. Gómez-Saiz, J. García-Torjal, M.A. Maestro, F.J. Arnaiz, T. Rojo, *Inorg. Chem.* 41 (2002) 1345.
- [49] G. Fernández, M. Corbella, G. Aullón, M.A. Maestro, J. Mahía, *Eur. J. Inorg. Chem.* (2007) 1285.
- [50] P.J. Hay, J.C. Thibeault, R. Hoffmann, *J. Am. Chem. Soc.* 97 (1975) 4884.
- [51] O. Kahn, *Molecular Magnetism*, VCH, New York, 1993. p. 131.
- [52] A.D. Naik, P.A.N. Reddy, M. Nethaji, A.R. Chakravarty, *Inorg. Chim. Acta* 349 (2003) 149.